Measurement of the Post-Combustion Residence Time in a Gas Turbine Aero-Engine

*†‡

JEFFREY HILTON MILES §¶

NASA John H. Glenn Research Center at Lewis Field, Cleveland, OH 44135

A challenging issue confronting the air transport system is the demand for the reduction of the emissions of oxides of nitrogen. NASA's Subsonic Fixed Wing (SFW) has set an aggressive goal in this area. The formation of thermal NO_x depends on the stoichiometry, the residence time linearly, and on the reaction temperature exponentially. Zeldovich thermalNO_x may be produced by oxidation of atmospheric nitrogen in the post flame gases. In the future, as turbine blade resistance to high temperatures improves nitrogen production in the post-combustion zone may become more important. While residence time is not as significant as temperature in formula predicting NO_x production, it is a necessary factor and should be as accurate as possible. The characteristic combustor residence time can be defined as the ratio of the combustor volume to the bulk (volumetric) flow rate. This value is estimated from geometry and operational data. However, detailed geometrical and operational data from gas turbine engine manufacturers is frequently unavailable. Furthermore, post-combustion residence time measurements are not available to verify analytical estimates. Consequently, in order to improve the technology to satisfy future emission prediction goals,

*extended abstract for a Gas Turbine Engine, Propellant and Combustion, or Aeroacoustic session

†extended abstract for the50th AIAA Aerospace Sciences Meeting 9 - 12 January 2012; Nashville, Tennessee

‡Abstract submission deadline: 01-June-2011

§Aerospace Engineer, Acoustics Branch,21000 Brookpark Road, Cleveland, Ohio, 44135

¶AIAA Associate Fellow

a different concept for determining the characteristic post-combustor residence time was investigated. The concept used is based on determining the post-combustion residence time delay due to convection of entropy at the flow speed in the combustor. It is evaluated from the slope of the combustor sensor signal/turbine exit signal pressure cross-spectrum phase angle over an appropriate frequency range where the measured signal can be attributed to indirect combustion noise. The procedure applied to a Honeywell TECH977 engine measured a post-combustion residence time near 4 ms at idle and 3.4 ms at a maximum power setting. Values at other power settings are discussed. The measurement of post-combustion residence time might have implications for fuel usage and system fault detection.

Nomenclature

E_{NO_x} NO_x emission index $gNO_2/kg - fuel$
f frequency, Hz
$\hat{G}_{x,x}(f)$ Estimated input signal one-sided auto spectral density function
$\hat{G}_{x,y}(f)$ Estimated one-sided cross-spectral density function
$\hat{G}_{y,y}(f)$ Estimated output signal one-sided autospectral density function
$H(f)$ Turbine frequency response (transfer) function
$H_s(f)$ System frequency response (transfer) function
K Turbine attenuation or producton/creation factor
$\dot{m}_{PZ}$ Mass flow in primary combustion zone,kg/s
M Mach number
m_f Fuel mass flow rate,kg/s
N_d Direct combustion noise signal system noise
N_i Indirect combustion noise signal system noise
N_{T} Tailpipe signal system noise
T Temperature, °K
$T_{AD,PZ}$ Adiabatic flame temperature
T_{inlet} Combustor inlet temperature, °K
T_m Mean temperature, °K
$U_{x,y}(f)$ aligned cross-spectral density function
V Volume of primary combustion zone,m^3
V_{pz} Volume of primary zone, m^3
$x(t)$ Input signal from combustor pressure sensor CIP1
$y(t)$ Output signal from turbine exit pressure sensor

Subscripts

10 Turbine exit signal, T551
11 Turbine exit signal, T552
3 Compressor exit - Combustor entrance
4 Combustor exit-Turbine inler
9 Combustor probe signal, CIP1
adiabatic Adiabatic
d Direct combustion noise
i Indirect combustion noise
x Input signal
y Output signal

Symbols

Measures contribution of direct combustion noise
ϕ Equivalence ratio
$\rho_{combair}$ Combustor air density, kg/m^3
τ_o indirect combustion noise time delay, ms

Superscripts

m measured

A Acoustic
E Estimated
H Hydrodynamic

I. Introduction

The National Aeronautics and Space Administration (NASA) has technology goals for future subsonic vehicles in the N+3 (2025) time frame to develop concepts to reduce NO_x better than 75 percent below the current standard of the Committee on Aviation Environment Protection (CAEP) while reducing aircraft fuel burn by better than 75 percent while achieving perceived cumulative noise levels 71 dB below stage 4 limits. Many of the reasons for the NO_x emission goals for flight vehicles are discussed in a report by Tengzelius.[1] A more general treatment of the theory of fixed and moving gas turbine including the topic of emissions as of 2001 is presentd by Saravanamuttoo et al.[2] A through treatment of gas turbine combustion and the topic of emissions as of 1999 is presented by Lefebvre.[3] Some of the research and application history of implementing NO_x control in land based gas turbines and boiler combustion chambers is discussed by Muzio and Quartucy.[4] The formation of thermal NO_x depends on the stoichiometry, the residence time linearly, and

on the reaction temperature exponentially. Zeldovich thermal NO_x may be produced by oxidation of atmospheric nitrogen in the post flame gases. In the future, as turbine blade resistance to high temperatures improves nitrogen production in the post-combustion zone may become more important. Syed[5] shows that the NO_x levels increase with increasing post-combustion residence time. The characteristic combustor residence time can be defined as the ratio of the combustor volume to the bulk (volumetric) flow rate. However, this type of turbofan engine data are considered to have a proprietary and sensitive status by an engine manufacturer. This has produced a lacuna of specific knowledge about the post combustion residence time in current and future combustor design concepts. For example, Wulff[6] states "residence times in turbofan combustors are of the order of magnitude of 5 ms." Consequently, in order to satisfy future emission goals, a different concept for determining the characteristic post-combustor residence time was investigated. The concept used is based on determining the post-combustion residence time delay due to convection of entropy at the flow speed in the combustor. It is evaluated from the slope of the combustor sensor signal/turbine exit signal pressure cross-spectrum phase angle over an appropriate frequency range where the measured signal can be attributed to indirect combustion noise.

Currently, low frequency noise generated in the turbofan engine core may make a significant contribution to the overall noise signature in the aft direction at the low power settings which are used on an airport flight approach trajectory. This type of low frequency noise may be a problem for future aircraft. Two possible low frequency noise sources are "direct" and "indirect" combustion noise. The source of combustion noise attributed to the unsteady pressures produced by the unsteady combustion process that propagate through the turbine to the far field is called the "direct" combustion noise source. The other source of turbofan engine combustion noise is known as the "indirect" mechanism in which the noise is generated in the turbine by the interaction of entropy fluctuations, which also originate from the unsteady combustion process, as they propagate through regions characterized by mean flow velocity or pressure gradients in the turbine stages. This indirect noise source was studied using analytical models by Ffowcs Williams and Howe,[7] Pickett,[8] Marble and Candel,[9] Cumpsty and Marble,[10,11] Cumpsty,[12] Gliebe et al.,[13] Mani,[14] Bodony[15] and Leyko[16] . Turbine noise was studied extensively in the 1970's. Studies were conducted on the topic of turbine tone generation. Other studies deal with the topic of attenuation of direct combustion noise. The topic of indirect combustion noise was studied analytically and in model scale tests. Indirect combustion noise was not thought to be a contributor to turbofan engine core noise. Consequently, studies of indirect combustion noise in turbofan engines were not conducted. A brief summary of some of this work is given in Appendix A. Presently, as a result of previous studies, core noise from turbofan engines is treated as being due to such individual sources as the compressor, combustor, and turbine. The turbine in previous

analytical and experimental studies has been treated as a device that attenuates the direct combustion noise with an attenuation constant that depends only on the turbofan engine operation parameters such as the pressure and temperature at the inlet and exit of the turbine and not on frequency.

The net travel time of the indirect combustion noise signal from the combustor to the turbine exit and the far field is increased since the travel velocity of the entropy fluctuations to the turbine is the flow velocity in the combustor. This flow velocity is a small fraction of the speed of sound. Miles et al.[17,18] has shown the pressure and entropy should be in phase in the combustor. Consequently, one might expect that the pressure signal from an indirect combustion noise source would be delayed relative to a pressure signal from a direct combustion noise source since an indirect combustion noise signal does not travel with the speed of an acoustic wave until it interacts with the turbine. Miles[19–21] with data from the Honeywell TECH 977 engine test program shows that the cross-spectra and correlation function between a combustor sensor and far-field microphones are tools that provides a way to separate "direct" and "indirect" coherent combustion noise due to this travel delay time. Further information is presented in Appendix B. Some of the other studies that used this set of data are discussed in Appendix C. This paper uses measurements in the combustor and turbine exit from the Honeywell TECH 977 engine test program to directly measure the post-combustion residence time. This paper uses tools that are part of signal-processing theory to study a combustor pressure sensor signal and a turbine exit pressure sensor signal. The cross-spectral density phase measurement identifies a time delay that corresponds to the convective time delay. The magnitude of the coherence between the two sensors identifies the spectral region of importance as being in the 50-250 Hz frequency range. This paper presents the cross-spectral density phase angle and the coherence over a range of operating conditions and calculates the post-combustion residence time from the slope of the cross-spectral density phase angle.

First expressions for NO_x emission and residence time will be discussed. In the following section, the engine noise data is discussed. Next, the linear system theory and a system model will be discussed. Then the post-combustion residence time results calculated from the cross-spectrum between a combustor pressure sensor and a turbine exit pressure sensor are presented. Finally, some conclusions are presented.

II. Estimation of NO_x production

Engine operation can be correlated with NO_x emission levels using regression analysis of measurable test parameters (T_3, T_4, P_3) or by consideration of time scales and chemical kinetics $(t_{res}, P_{comb}, T_{adiabatic})$ or using both sets of variables along with such variables as

equivalence ratio, fuel flow rate and Mach number. In this section the use of the primary zone residence time in the estimation of NO_x production will be examined.

A. NO_x production for a Propane Air Combustion

A 1978 correlation of NO_x emission levels determined by Roffe and Venkataramani[22,23] for propane air combustion is based only on the residence time and adiabatic flame temperature. They determined NO levels for their experiment are principally a function of adiabatic flame temperature and combustor residence time. This function is represented by the expression

$$E_{NO_x} = t_{res}\ \exp\left\{-72.28 + 2.80\sqrt{T_{adiabatic}} - \frac{T_{adiabatic}}{38.02}\right\} \tag{1}$$

where E_{NO_x} is the NO_x emission index ($gNO_2/kg - fuel$), $T_{adiabatic}$ is the adiabatic flame temperature (°K) and τ_{res} is the combustor residence time (ms). They found that over the range of pressures from 5 to 30 atmospheres, there is no significant observed departure from this expression for inlet temperatures 727K and higher. In the next section some definitions of primary zone residence time are discussed.

III. Primary zone residence time

According to a 2002 paper by Spadaccini et al[24] the characteristic combustor residence time is given by the bulk flow through the combustor volume

$$\tau_{residence} = \frac{volume}{volumetricflowrate} = \frac{VP}{mRT} \tag{2}$$

Spadaccini et al[24] states ≈ 7 ms is the residence time in a conventional combustor and ≈ 0.5 ms for a micro-combustor.

Another equation for calculating the primary combustion zone residence time used by R⊘kke et al.[25] in a 2003 paper is

$$\tau_{PZ} = \frac{V_{PZ}\ \rho_{combair}}{\dot{m}_{PZ}}\ \frac{T_{inlet}}{T_{AD,PZ}} \tag{3}$$

In examining a set of exemplified gas turbine dual fuel, dry low emission combustion system R⊘kke et al.[25] found primary zone residence times of 2.71, 1.35,8.17,4.09, 9.84, and 4.92 ms.

A. Gas Turbine NO_x production

Gas turbine NO_x production as explained by Lefebvre[26] in a 1984 article is more complicated than NO_x emission from a propane combustor since in addition to the resident time dependence

1. The reaction rate is assumed to be a function of pressure in addition to temperature

$$\text{reaction rate} = P^m \exp(zT) \tag{4}$$

2. The mixing rates are assumed to be a function of linear pressure drop

$$\text{mixing rate} = \left(\frac{\Delta P}{P}\right)^x \tag{5}$$

Consequently,

$$\begin{aligned} E_{NO_x} &= A \left(\frac{P\,V}{\dot{m}_A\,T}\right) \left(\frac{\Delta P}{P}\right)^x P^m \exp(zT) \\ &= \frac{A\,V_c\,(\Delta P)^x\,P^{(1+m-x)} \exp(zT)}{\dot{m}_A\,T} \end{aligned} \tag{6}$$

Lefebvre[26] correlated a large set of engine data using $A = 9 \times\ 10^{-8}$, $x = 0$, $m = 0.25$, and $z = 0.01$ so that

$$E_{NO_x} = \frac{9.0 \times\ 10^{-8}\ V_c P_3^{1.25} \exp(0.01\ T_{st})}{\dot{m}_A\ T_{pz}} \tag{7}$$

In 1993 Rizk and Mongia[27] recast Lefebre's expression 7 and made changes to improve correlation with data and derived

$$E_{NO_x} = \frac{1.5 \times\ 10^{15}\ (\tau_{NO_x} - 0.5\ \tau_{ev})^{0.5} \exp(-71100/T_{St})}{P_3^{0.05}\,(\Delta P_3/P_3)^{0.5}} \tag{8}$$

where $\tau_{\mathrm{NO_x}}$ is the residence time in the $\mathrm{NO_x}$ production region, τ is the evaporation time, T_{St} is the reaction temperature, P_3 is the combustor inlet pressure, and $(\Delta P_3/P_3)$ is the combustor pressure drop.

Consequently, the primary zone residence time has evolved to become a $\mathrm{NO_x}$ emission production parameter evaluated by doing a least squared curve fit to a large data set. The primary zone residence time formulation has become more complex as combustor design has become more complex. In part, this may be due to it not being a measurable quantity. When used as correlation factor it should be referred to as a primary zone $\mathrm{NO_x}$ emission residence time and not as the primary zone residence time. In this paper, a procedure to measure the post-combustion residence time using signal processing methods is discussed. As a consequence, this post-combustion/post-flame residence time becomes available for consideration with knowledge of any engine company proprietary combustor geometry design information or proprietary operating parameters.

IV. Engine Noise Data and Analysis

A. Engine test data

The NASA/Honeywell static engine test program was conducted at Honeywell's San Tan outdoor acoustic test facility using a Honeywell TECH977 engine (Fig. 2) and the results are described in a report by Weir.[28] The dual-spool, turbofan engine has a direct drive, wide chord fan connected by a long shaft to the low-pressure turbine spool and a high-pressure compressor connected by a concentric short shaft to the turbine high-pressure spool. The fan diameter is 34.2 in. The combustor design is a straight-through-flow annular geometry with 16 fuel nozzles and 2 igniters. Data obtained for one configuration in the test program is analyzed in this paper. The engine-internal instrumentation in this configuration included high-temperature pressure sensors with air cooling in a combustor igniter port identified herein as CIP1 (sensor 9) and at the turbine exit sensors identified as T551 (sensor 10) and T552 (sensor 11). Pressure time histories at these internal sensors are used herein.

The data acquisition system had a sampling rate of 65 536 Hz and a sampling duration of roughly 70 s. The spectra were calculated using a 50 percent overlap. This permitted data reduction using ≈ 254 overlapped ensemble averages at a bandwidth resolution of 2 Hz. Further signal estimation parameters are shown in Table 1.

Table 1. Spectral estimate parameters.

Parameter	Value
Segment length, (data points per segment), N	32 768
Sample rate, r_s, samples/s	65 536
Segment length, $T_d = N/r_s$, s	0.500
Sampling interval, $\Delta t = 1/r_s$, s	1/65 536
Bandwidth resolution, $B_e = \Delta f = 1/T_d = r_s/N$, Hz	2.0
Upper frequency limit, $f_c = 1/2\Delta t = r_s/2$, Hz	32 768
Propagation time delay/lag ($T = 9^o$C,$r = 30.48$ m) $\tau_P = 5\ 927/65\ 536$, s	0.09044
Number of independent samples, n_s	128
Overlap	0.50
Sample length, T_{total}, s	≈ 70

B. Combustor-Turbine Exit Acoustics

All the spectra and cross-spectra are estimated using Welch's nonparametric method which is based on averaging multiple windowed periodograms using overlapping time sequences.[29–33] Using these spectra and cross spectra, the magnitude squared coherence is calculated to measure the similarity of the amplitude variations at particular frequencies.[33] The $\hat{}$ accent

will be used to denote the statistical basis of a variable. This is done to avoid confusion with calculations of coherence using a single segment or block which yield a coherence of unity.

The concept used is based on determining the post-combustion residence time delay due to convection of entropy at the flow speed in the combustor identified by Miles.[19,20] It is evaluated from the slope of the combustor sensor signal/turbine exit signal pressure cross-spectrum phase angle over an appropriate frequency range where the measured signal can be attributed to indirect combustion noise.

The appropriate frequency range is determined from the combustor sensor signal/turbine exit signal magnitude squared aligned coherence (MSC) function. Figures 3–9 using sensors 9 and 10 and figures 10–16 using sensors 9 and 11 show the MSC function as part (a) and the cross-spectrum phase angle as part (b).

Plots using a logarithmic MSC function scale are presented. The MSC function is given by

$$\hat{\gamma}^2_{x,y} = \frac{|\hat{G}_{x,y}|^2}{\hat{G}_{x,x}\hat{G}_{y,y}} \tag{9}$$

Also shown in part (a) of Figs. 3–9 are coherence threshold calculated from

$$\hat{\gamma}^2_{x_n x_n}(n_s) = 1 - (1-P)^{1/(n_s-1)} \tag{10}$$

where this formula determines a P-percent threshold confidence interval using the number of data segments/blocks, n_s, used in the Welch's periodogram method spectral estimator. (see Miles[34]). The 95 percent confidence interval based on $n = 128$ independent samples is 0.0233. The spectra are calculated using a 50 percent overlap and the 95 percent confidence interval based on $n = 273$ samples is 0.0109. These indicators show the MSC function is reliable up to about 400 Hz. However, MSC function is above 0.1 only in a region from $30 - 250$ Hz. The phase angle variation in this region is attributed to indirect combustion noise.

Miles[34] shows that instead of relying on the confidence interval given by Eq. (10), which is based on a statistical theory, to obtain a threshold value for $\hat{\gamma}^2_{nn}(n_s)$, one can use a deliberately unaligned time history to create the threshold value. If one of the time histories is shifted by a time delay more than the segment/block length, $T_d = N/r_s$, then the two time histories are totally independent unless tones are present. This deliberate decorrelation establishes a coherence threshold and also identifies any tones in the signals. Shifting the signals by this time delay removes the coherence of random noise but leaves the coherence of periodic functions which are sometimes identified as hidden periodicities, concealed spectral lines, or undamped sinusoids in noise. The deliberately unaligned coherence is also shown in part (a) of Figs. 3–9. Note that the higher statistical confidence interval based on the

number of independent records ($n_d = 128$) is a more conservative estimate of the measured coherence threshold. The statistical coherence threshold can be used with confidence since it can be compared with a measured coherence threshold. The coherence value is below the 95 percent statistical confidence interval above 400 Hz. Consequently, this is the upper frequency limit for which data is available for analysis using a linear system model.

V. Linear System Theory

The methods used herein are based on system theory developed for linear systems with random inputs as discussed by Bendat and Piersol[35–37] Candy[38] and Manolakis et al.[33] . In this paper the linear system theory discussed is in the frequency domain. The output spectral density function, $\hat{G}_{y,y}$, and the cross-spectra density function, $\hat{G}_{x,y}$, is related to an input spectral density function, $\hat{G}_{x,x}$, through frequency response function, $H_{x,y}(f)$, representing the turbine as

$$\hat{G}_{y,y} = |H_{x,y}(f)|^2 \hat{G}_{x,x} \tag{11}$$

and

$$\hat{G}_{x,y} = H_{x,y}(f)\hat{G}_{x,x}. \tag{12}$$

where x is the input signal from the combustor pressure sensor CIP1 and y is the output signal from one of the turbine exit pressure sensors.

The cross spectral density and the frequency response functions are complex valued quantities, which can be expressed in terms of a magnitude and an associated phase angle. This will be expressed herein using complex polar notation.

$$\hat{G}_{x,y}(f) = |\hat{G}_{x,y}(f)| \exp\left[-j\hat{\phi}(f)\right] \tag{13}$$

$$H_{x,y}(f) = |H_{x,y}(f)| \exp\left[-j\psi(f)\right] \tag{14}$$

Before plotting the cross spectral density phase angle, phase unwrapping is applied to the phase angle to avoid a jump of 2 π in the phase caused by the ATAN2 function[30](Chapter 14.3,pages 295–297).

The system under consideration has a combustion noise input with a measured spectrum, $G^m_{9,9}(f)$, which includes acoustic and hydrodynamic components. The system measured output quantities are assumed to be related as follows:

$$\hat{G}^m_{9,10}(f) = H^m_{9,10}(f)\,\hat{G}^m_{9,9}(f) \quad (15)$$

$$\hat{G}^m_{10,10}(f) = |H^m_{9,10}(f)|^2\,\hat{G}^m_{9,9}(f) \quad (16)$$

and the measured MSC

$$\hat{\gamma}^2_{9,10} = \frac{|\hat{G}^m_{9,10}|^2}{\hat{G}^m_{9,9}\,\hat{G}^m_{10,10}} \quad (17)$$

where ^{m} indicates noise may be included in the measured quantities. Only measurements with the combustor sensor, $CIP1(9)$ and turbine exit sensor, $T551(10)$, are discussed herein. The unknown that will be identified is the turbine frequency response function, $H^m_{9,10}(f)$ at a range of operating conditions.

VI. Model equations

The system model discussed in this section is applied in the 50-250 Hz frequency range. The model involves the turbine attenuation and the convective time delay of the of the entropy signal. The plant being modeled is the turbine. The input to the plant is the total pressure signal and the measurement made in the combustor is of the total pressure signal. Consequently, the available input auto-spectrum is that of the total pressure signal. To aid in physical interpretation, a standard template parametric model form will be used. The model form examined in this paper is in a parametric reduced order frequency domain representation. The parameters depend nonlinearly on the operating point. However, at each operating condition the system will be assumed to be linear and the same parametric form will be used so that source separation will be obvious. The nonlinear operation is then described by a linear model at a range of observed operating points each identified by a set of parameters. This paper discusses measurements at the 48, 54, 60, 87 percent maximum power settings and at two maximum power settings. Over the frequency range 50-250 Hz, the turbine exit signal will be the' result of an attenuation of the input signal by an amount K. At the turbine exit, the input signal will also have a time delay since the indirect combustion noise travels at the flow velocity.

t

Consider an input signal $x(t)$ with a spectrum $G_{x,x}(f)$ for a system with transfer function $H_{x,y}(f)$ and output signal $y(t)$. Then the cross spectrum is given by Eq. (12). For the turbofan engine the input to the turbine is is the direct acoustic signal $x_d(t)$ and the time delayed entropy signal, $x_i(t)$, with a delay of τ_o. The entropy signal may represent in

addition to a temperature fluctuation moving with the flow any other disturbance moving with the flow such as a vorticity fluctuation. A Turbine-Combustor-Tailpipe Noise system diagram is shown in Fig. 1.

The system model is constructed as follows. The output turbine noise signals are $y_d(t)$ and $y_i(t)$ as shown in Fig. 1.

The output signal, y, is the sum of the direct combustion noise signal, y_d, and the indirect combustion noise signal, y_i.

$$y = y_i \tag{18}$$

The direct combustion noise cross-spectral density, $G_{x_d y_d}$, is a product of the direct combustion noise turbine transfer function, $H_d(f)$, and the direct combustion noise input spectral density, G_{x_d}.

$$G_{x_d y_d} = H_d(f) G_{x_d} \tag{19}$$

The indirect combustion noise cross-spectral density, $G_{x_d y_i}$, is a product of the indirect combustion noise turbine transfer function, $H_i(f)$, the time delay factor, $e^{-j\,2\,\pi\,f\tau_o}$, and the input indirect combustion noise spectral density, G_{x_i} which corresponds to an equivalent fluctuating entropy spectral density function.

$$G_{x_d y_i} = H_i(f) e^{-j\,2\,\pi\,f\tau_o} G_{x_i} \tag{20}$$

The indirect combustion noise turbine transfer function, $H_i(f)$, is assumed to have a representation, $H(f)$. The direct combustion noise turbine transfer function, $H_d(f)$, is assumed to have a representation, $\alpha\, H(f)$. Where α is a measure of the direct combustion noise to the indirect combustion noise.

$$H_d(f) = \alpha H(f) \tag{21}$$

$$H_i(f) = H(f) \tag{22}$$

The direct combustion noise and the entropy noise have the same origin in the combustion process. Consequently it is assumed that the input direct combustion noise spectral density and the input entropy fluctuation spectral density have the same form.

$$G_{x_d} = G_{x_i} \tag{23}$$

Consequently, the measured cross-spectral density is given by

$$
\begin{aligned}
G_{x_d,y} &= G_{x_d y_d} + G_{x_d y_i} = H_d(f) G_{x_d} + H_i(f) G_{x_i} \\
&= H(f)(e^{-j\,2\,\pi\,f\tau_o} + \alpha) G_{x_d} = H_s(f) G_{x_d}
\end{aligned} \tag{24}
$$

For the frequency range 50-250 Hz, α is negligible and $H(f) = K$where $log_{10}(K) \approx -10$.

Consequently, the transfer function of the system is

$$
H_s(f) = K e^{-j\,2\,\pi\,f\tau_o} \tag{25}
$$

The combustor entropy noise, N_i, and combustor hydrodynamic noise, N_d, are assumed independent of each other and independent of the tailpipe noise, N_T.

$$
G_{N_i N_d} = G_{N_i N_T} = G_{N_d N_T} = 0
$$

VII. Results

Table 2. Linear fit values(09-10)

Percent Maximum Power	a ms	b Degrees	Correlation	Std. Dev. ms
48	3.99	-78.06782	0.985	0.0701
54	3.86	-79.9248	0.982	0.0746
60	4.0229	-90.7813	0.974	0.0942
71	3.7079	-75.56375	0.97	0.093
87	3.4814	-83.738	0.948	0.117
98	3.99	-78.0678	0.985	0.07
99	3.3435	-83.024	0.944	0.117

A linear curve fit covering the frequency range from 50-250 Hz was made to the cross-spectrum phase angle for the measurement made using the combustor pressure sensor and a turbine exit pressure sensor . The linear curve fit results based on using sensor 9 and 10 are shown in table 2 and the linear curve fit results based on using sensor 9 and 11 are shown in table 3. The post-combustion residence times are shown in Fig. 17 for each power setting and microphone pair. The measured a post-combustion residence time was near 4 ms at idle and 3.4 ms at a maximum power setting. The sensor pairs do not behave identically at each

Table 3. Linear fit values (09-11)

Percent Maximum Power	a ms	b Degrees	Correlation	Std. Dev. ms
48	4.024	-77.3482	0.986	0.0687
54	4.079	-84.048	0.985	0.071
60	4.0664	-83.6347	0.986	0.0683
71	4.0188	-90.96	0.966	0.108
87	3.5794	-83.3152	0.961	0.104
98	3.5477	-88.01	0.958	0.107
99	3.57	270.46	0.966	0.096

power setting.

VIII. Discussion

A. Post-Primary Zone NO_x

In a review of NO_x formation in gas-turbine combustors Correa[39] indicated NO_x is formed in a distributed zone manner and that higher temperature-rise combustors will be required as turbine materials improve. While most correlation of NO_x production equations apply in the primary zone, research has been conducted to find equations for other zones. A NO_x production equation for the lean zone is given by Rizk and Mongia.[40]

B. System verses components

The findings presented herein a based on a combustor/turbine system study. Studying each component separately does not lead to these findings.

C. Engine aging

Lukachko and Waits[41] mention in a discussion of engine aging that using a constant thrust power setting a decrease in NO emissions as a function of engine age is observable. This is attributed to an increase in mass flow due to hot section damage. They suggest that turbine damage results in lower NO_x emissions rate due to decreased residence time. Consequently, the post-combustion residence time measurement procedure might be used to detect turbine damage from aging or verify proper operation.

The typical fault diagnostic turbine system sensor system depends on measuring such items as fan exit pressure, LPC exit pressure, Burner pressure, LPC exit temperature, HPC

exit temperature, Exhaust gas temperature, fuel flow, Low spool speed, and high spool speed.[42–46] None of these items convey the same information as the combustor residence time which is a function of the turbine blade system operating condition and geometry. The available time to take corrective or compensatory actions such as repair or replace a part or reduce system operational loads to extend the life of the faulted part might be reduced with additional information.

A gas turbine engine in a military or commercial aero-engine, or in industrial environment is a safety-critical system which needs real-time fault detection and a decision support system to advise corrective actions so that the system can continue to function without jeopardizing the safety of personnel or damage to the equipment involved. Information on the status of the post-combustion residence time can provide additional information not available from any current sensor used in current fault detection systems. In addition, jet fuel costs are 30 percent of an airlines cost. The status of post-combustion resident time as a function of time might provide information related to fuel usage.

IX. Conclusions

The post-combustion residence time was measured as a function of engine power. For this turbofan engine the post-combustion residence time was near 4 ms at idle and 3.4 ms at a maximum power setting

The measurement of post-combustion residence time might have implications for fuel usage and system fault detection.

X. Acknowledgment

This work was supported by the NASA Fundamental Aeronautics Subsonic Fixed Wing program.

A. Turbine noise studies

In the 1970's the turbine tone noise topic became important and descriptions of the turbine tone behavior and empirical turbine noise prediction models using engine operating parameters were published by Fletcher and Smith,[47] Mathews and Peracchio,[48] Kazin and Matta,[49] Mathews et al.[50] and Krejsa and Valerino.[51] In the 1970's turbine operating parameters also became an important part of many empirical jet engine direct combustion noise prediction schemes, which needed a turbine transmission loss coefficient. Transmission of sound through turbines was studied experimentally using a component test procedure

by Doyle and Matta,[52] and using a CF6-50 turbofan engine by Doyle[53] and by Doyle and Moore.[54] A theoretical physics based model of low frequency noise transmission through turbines is discussed by Matta and Mani.[55] Prediction procedures are also presented by for example Huff et al.,[56] Motsinger and Emmerling,[57] Mathews and Rekos,[58] Mathews et al.,[59] and Anon.[60] These prediction procedures are independent of frequency and provide a loss factor for the combustion noise. This paper will examine turbine transmission loss by modeling a frequency dependent turbine acoustic transfer function.

B. Separation of indirect and direct combustion noise

The core noise components of the dual-spool turbofan engine were separated by Miles[19] using coherence functions. A source location technique was used that adjusted the time delay between the combustor pressure sensor signal and the far-field microphone signal to maximize the coherence and remove as much variation of the phase angle with frequency as possible. For the 130^o far-field microphone, a 90.03 ms time shift worked best for the frequency band from 0-200 Hz, while an 86.98 ms time shift worked best for the frequency band from 200-400 Hz. Hence, the 0-200 Hz band signal took more time than the 200-400 Hz band signal to travel the same distance. This suggests the 0-200 Hz coherent cross spectral density band is partly due to indirect combustion noise attributed to entropy fluctuations, which travel at a low flow velocity in the combustor until interactions with the turbine pressure gradient produce indirect combustion noise. The signal in the 200-400 Hz frequency band is attributed mostly to direct combustion noise. The method is successful because acoustic and temperature fluctuations were found by Miles[17,18] to be related by a linear transfer function that includes a convective time delay. This experiment involved the measurements of pressure and temperature disturbances in a long tube connected to a combustor. This linear connection of entropy and pressure fluctuations implies the direct and indirect combustion noise are correlated at the source. This measurement of a convective entropy correlation with acoustic pressure by Miles is also discussed by Mahan and Karchmer.[61]

C. Honeywell TECH977 studies

In this paper, results of a study of auto-spectra and cross-spectra measured using a sensor in the combustor and two sensors at the turbine exit of a Honeywell dual-spool TECH977 turbofan engine are reported. Acoustic data from the same TECH977 engine test program are discussed by Nance,[62] Gaeta et al.,[63] Alonso et al.,[64] Miles,[19–21] Mendoza et al.,[65] Weir and Mendoza,[66] Schuster,[67] Royalty and Schuster,[68] Dougherty and Mendoza,[69,70] Weir,[28] and Hultgren and Miles.[71] The research discussed is an extension of the study of

the combustion noise of the TECH977 engine conducted by Miles,[19] using a coherent output power spectral domain coherence function procedure and the generalized cross-correlation function procedure used by Miles.[20,21]

References

[1]Tengzelius, U., "NOx Emissions and Engine Performance Results for Studied Engine Concepts including final Summary," Tech. Rep. FOI-R-3026–SE, FOI, Swedish Defense Research Agency, 2010.

[2]Saravanamuttoo, H. I. H., Rogers, G. F. C., and Cohen, H., *Gas Turbine Theory: 5th Edition*, Pearson Education, 2001, pages 290–301.

[3]Lefebvre, A. H., *Gas Turbine Combustion: 2nd Edition*, Taylor & Francis, New York, 1999, pages 311-283.

[4]Muzio, L. J. and Quartucy, G. C., "Implementing NOx Control: Research to Applications," *Progress in Energy and Combustion Science*, Vol. **23** No., 1997, pp. 233–266.

[5]Syed, K. J., Roden, K., and Martin, P., "A Novel Approach to Predicting NOx Emissions from Dry Low Emissions Gas Turbines," GT2006-90333, Proceedings of the GT2006 ASME Turbo Expo 2006:Power for Land, Sea, and Air, May 8-11, 2008, Barcelona, Spain, May 2006.

[6]Wulff, A. and Hourmouziadis, J., "Technology Review of Aeroengine Pollutant Emissions," *Aerospace Science and Technology*, Vol. **8** No., 1997, pp. 557–572.

[7]Williams, J. E. F. and Howe, M. S., "The generation of sound by density inhomogeneities in low Mach number nozzle flows," *J. Fluid Mech.*, Vol. **70** Part 3, 1970, pp. 605–622.

[8]Pickett, G. F., "Core Engine Noise Due to Temperature Fluctuating Through Turbine Blade Rows," Tech. Rep. AIAA-75-528, AIAA, 1975.

[9]Marble, F. E. and Candel, S. M., "Acoustic disturbance from gas non-uniformities convected through a nozzle," *Journal of Sound and Vibration*, Vol. **55** No. 2, 1977, pp. 225–243.

[10]Cumpsty, N. A. and Marble, F. E., "The Interaction of Entropy Fluctuations With Turbine Blade Rows; A Mechanism of Turbojet Noise." *Proc. R. Soc. Lond. A.*, Vol. **357**, 1977, pp. 323–344.

[11]Cumpsty, N. A. and Marble, F., "Core Noise from Gas Turbine Exhausts," *Journal of Sound and Vibration*, Vol. **54** No. 2, 1977, pp. 297–309.

[12]Cumpsty, N. A., "Jet Engine Combustion Noise: Pressure, Entropy and Vorticity Perturbations Produced by Unsteady Combustion or Heat Addition," *Journal of Sound and Vibration*, Vol. **66** No. 4, 1979, pp. 527–544.

[13]Gliebe, P., Mani, R., Shin, H., Mitchell, B., Ashford, G., Salamah, S., and Connell, S., "Acoustic Prediction Codes," Tech. Rep. NASA CR–2000-210244, R99AEB169, General Electric Aircraft Engines, August 2000.

[14]Mani, R., "Issues in Combustion Noise," Annual Research Briefs 2007, Center for Turbulence Research, Department of Mechanical Engineering , Stanford University Stanford, Ca, 94305,USA, 2007, `http://ctr.stanford.edu/ResBriefs07/22_mani_pp255_264.pdf`

[15]Bodony, D. J., "Scattering of an entropy disturbance into sound by a symmetric thin body," *Physics of Fluids*, Vol. **21** , 2009, pp. 096101–1–10.

[16]Leyko, M., Nicoud, F., and Poinsot, T., "Comparison of Direct and Indirect Combustion Noise Mechanisms in a Model Combustor," *AIAA Journal*, Vol. No., November 2009, pp. 2709–2716.

[17]Miles, J. H., Wasserbauer, C. A., and Krejsa, E. A., "Cross Spectra Between Temperature and Pressure in a Constant Area Duct Downstream of a Combustor," AIAA-83-0762, NASA TM-83351, 1983.

[18]Miles, J. H., Wasserbauer, C. A., and Krejsa, E., "Cross spectra between pressure and temperature in a constant-area duct downstream of a hydrogen-fueled combustor," Tech. Rep. NASA-TM-83463, NASA Glenn Research Center, 1983.

[19]Miles, J. H., "Time Delay Analysis of Turbofan Engine Direct and Indirect Combustion Noise Sources," *Journal of Propulsion and Power*, Vol. **25** No. 1, January-February 2009, pp. 218–227.

[20]Miles, J. H., "Core Noise Diagnostics of Turbofan Engine Noise Using Correlation and Coherence Functions," *Journal of Propulsion and Power*, Vol. **26** No. 2, March/April 2010, pp. 303–316.

[21]Miles, J. H., "Separating Direct and Indirect Turbofan Engine Combustion Noise Using the Correlation Function," *Journal of Propulsion and Power*, Vol. **26** No. 5, September–October 2010, pp. 1144–1152.

[22]Roffe, G. and Venkataramani, K. S., "Experimental Study of the Effects of Cycle Pressure on Lean Combustion Emissions," Tech. Rep. NASA CR-3032, NASA, 1978.

[23]Roffe, G. and Venkataramani, K. S., "Emission measurements for a lean premixed propane/air system at pressures up to 30 atmospheres," Tech. Rep. NASA CR-159421, NASA, 1978.

[24]Spadaccini, C. M., Lee, J., Lukachko, S., Waitz, I. A., Mehra, A., and Zhang, X., "High Power Density Silicon Combustion Systems for Micro Gas Turbine Engines," GT-2002-30082, Proceedings of ASME TURBO EXPO 2002, Amsterdam, The Netherlands, June 2002, 2002.

[25]R⊘kke, P. E., Hustad, J. E., R⊘kke, N. A., and Svendsgaard, O. B., "Technology Update on Gas Turbine Dual Fuel, Dry Low Emission Combustion Systems," ASME GT-2003-38112, ASME Turbo Expo 2003 June 16-19, 2003, Atlanta, USA, June 2003.

[26]0Lefebvre, A. H., "Fuel Effects for Gas Turbine Combustion-Liner Temperature, Pattern Factor, and Pllutant Emissions," *J. Aircraft*, Vol. **21** No. 11, November 1984, pp. 887–898.

[27]Rizk, N. K. and Mongia, H. C., "Semianalytical Correlations for NOx, CO, and UHC Emissions," *J. Eng. Gas Turbines Power*, Vol. **115** No. 3, July 1993, pp. 612–619.

[28]Weir(editor), D. S., "Engine Validation of Noise & Emission Reduction Technology Phase 1," Tech. Rep. NASA/CR-2008-215225, Honeywell, May 2008.

[29]Welch, P. D., "The Use of Fast Fourier Transform for the Estimation of Power Spectra: A Method Based on Time Averaging Over Short, Modified Periodograms," *IEEE Transactions on audio and electroacoustics*, Vol. **AU-15** No.2, June 1967, pp. 70–73.

[30]Stearns, S. D. and David, R. A., *Signal Processing Algorithms Using Fortran and C*, Prentice-Hall, Inc., 1993.

[31]Porat, B., *Digital Processing of Random Signals*, Dover Publications, NY, 1994,2008.

[32]Hayes, M. H., *Statistical Digital Signal Processing and Modeling*, John Wiley & Sons, 1996.

[33]Manolakis, D. G., Ingle, V. K., and Kogon, S. M., *Statistical and Adaptive Signal Processing*, Artech House, Boston, Massachusetts and London, United Kingdom, 2005.

[34]Miles, J. H., "Aligned and Unaligned Coherence: A New Diagnostic Tool," Tech. Rep. AIAA-2006-0010, AIAA, 2006, Presented at the 44th AIAA Aerospace Science Meeting, 9-12 Jan 2006 Reno Hilton Reno, Nevada, also NASA/TM–2006-214112.

[35]Bendat, J. S. and Piersol, A. G., *Measurement and Analysis of Random Data*, John Wiley & Sons, 1966.

[36]Bendat, J. S. and Piersol, A. G., *Random Data: Analysis and Measurement Procedures*, John Wiley & Sons, 1971.

[37]Bendat, J. S. and Piersol, A. G., *Engineering Applications of Correlation and Spectral Analysis*, John Wiley & Sons, 1980.

[38]Canday, J. V., *Signal Processing. The Modern Approach.*, McGraw-Hill, New York, 1988.

[39]Correa, S. M., "A Review of NO_x Formation Under Gas-Turbine Combustion Conditions," *Combustions Science and Technology*, Vol. **87** No., 1992, pp. 329–362.

[40]Rizk, N. K. and Mongia, H. C., "Emissions Predictions of Different Gas Turbine Combustors," AIAA-94-0118, 1994.

[41]Lukachko, S. P. and Waitz, I. A., "Effects of Engine Aging on Aircraft NOx Emissions," ASME 97-GT-386, presented at the Inaternational Gas Turbine and Aeroengine Congress, Orlando, Florida –June 2-5, 1997, June 1997.

[42]Brown, M. N., Stewart, R. W., Durrani, T. S., and Buggy, T. W., "DSP subsystem for knowledge based health monitoring of gas turbine engines," 1992 IEEE International Conference on Acoustics, Speech, and Signal Processing, 23-26 March 1992, San Francisco, CA, March 1992.

[43]Ashby, M. J. and Scheuren, W. J., "Intelligent maintenance advisor for turban engines," 2000 IEEE Aerospace Conference Proceedings, Vol. 6, 211–219, 18–25 Mar 2000, Big Sky, MT, March 2000.

[44]Roemer, M. J. and Kacprzynski, G. J., "Advanced Diagnositcs and Prognostics for Gas Turbine Engine Risk Assessment," 2000 IEEE Aerospace Conference Proceedings, Vol. 6, 345–353 18–25 Mar 2000, Big Sky, MT, March 2000.

[45]Kodali, A., Vemana, S., Choi, K., Pattipati, K., Namburu, S. M., Prokhorov, D. V., and Qiao, L., "Diagnostic Ambiguity and Parameter Optimization in Classifier Fuision: Application to Gas Turbine Engine Data," 2008 IEEE Autotestcom, 8-11 Sept 2008, Salt Lake City, UT, 433–438, September 2008.

[46]Donat, W., Choi, K., An, W., Singh, S., and Pattipati, K., "Data Visualization, Data Reduction and Classifier Fusion for Intelligent Fault Diagnosis in Gas Turbine Engines," *Journal of Engineering for Gas Turbines and Power*, Vol. **130** No., July 2008, pp. 041602(1–8).

[47]Fletcher, J. S. and Smith, P. H., "The Noise Behaviour of Aero Engine Turbine Tones," AIAA-1975-466, March 1975.

[48]Mathews, D. C. and Peracchio, A. A., "Proagress in Core Engine and Turbine Noise Technology," AIAA-1974-948, August 1974.

[49]Kazin, S. B. and Matta, R. K., "Turbine Noise Generation, Reduction and Prediction," AIAA-1975-449, March 1975.

[50]Mathews, D. C., Nagel, R. T., and Kester, J. D., "Review of Theory and Methods for Turbine Noise Prediction," AIAA-1975-540, March 1975.

[51]Krejsa, E. A. and Valerino, M. F., "Interim Prediction Method for Turbine Noise," Tech. Rep. NASA TM-X-73566, NASA, 1976.

[52]Doyle, V. L. and Matta, R. K., "Attenuation of upstream-generated low frequency noise by gas turbines," Tech. Rep. NASA-CR-135219, NASA, 1977.

[53]Doyle, V. L., "Experimental clean combustor program, phase 3 Noise measurement addendum," Tech. Rep. NASA-CR-159458; R78AEG319, General Electric Company, Cincinnati, OH, 1978, Contract-Grant-Task Number: NAS3-19736.

[54]Doyle, V. L. and Moore, M. T., "Core Noise Investigation of the CF6–50 Turbofan Engine, Final Report," Tech. Rep. R79AEG395, NASA CR–159749, General Electric Company, Cincinnati, OH, Jan. 1980, Contract-Grant-Task Number: NAS3–21260.

[55]Matta, R. K. and Mani, R., "Theory of low frequency noise transmission through turbines," Tech. Rep. NASA-CR-159457, NASA, 1979.

[56]Huff, R. G., Clark, B. J., , and Dorsch, R. G., "Interim Prediction Method for Low Frequency Core Engine Noise," Tech. Rep. NASA TM X-71627, NASA Glenn Research Center, 1974.

[57]amd J. J. Emmerling, R. E. M., "Review of theory and methods for combustion noise prediction," AIAA-1975-541, March 1975.

[58]Mathews, D. C. and Rekos Jr., N. F., "Prediction and Measurement of Direct Combustion Noise in Turbopropulsion Systems," *J. Aircraft*, Vol. **14** No.9, September 1977, pp. 850–859.

[59]Mathews, D. C., Rekos, Jr., N. F., and Nagel, R. T., "Combustion Noise Investigation," Tech. Rep. FAA-RD-77-3, PWA-5478, FAA Report, 1977.

[60]anon, "GAS Turbine Jet Exhaust Noise Prediction," Tech. Rep. ARP876, SAE, 1978.

[61]Mahan, J. R. and Karchmer, A., "Combustion and Core Noise," *Aeroacoustics of Flight Vehicle Theory and Practice*, edited by H. H. Hubbard, chap. 9, NASA Reference Publication 1258, Vol. 1 WRDC Technical Report 90-3052, August 1991, pp. 483–517.

[62]Nance, D. K., *Separating Contributions of Small-Scale Turbulence, Large-Scale Turbulence, and Core Noise from Far-Field Exhaust Noise Measurements*, Ph.d dissertation, Georgia Institute of Technology, 2007.

[63]Gaeta, R. J., Mendoza, J. M., and Jones, M. G., "Implementation of In-Situ Impedance Technique on a Full Scale Aero-Engine System." AIAA-2007-3441, 2007.

[64]Alonso, J., Kwan, H.-W., and Burdisso, R., "EVNERT Program: Testing of Adaptive HQ-Liner for Aft Noise Control," AIAA-2008-2811, May 2008, 14th AIAA/CEAS Aeroacoustics Conference (29th AIAA Aeroacoustics Conference), Vancouver, British Columbia, May 5-7, 2008.

[65]Mendoza, J. M., Nance, D. K., and Ahuja, K. K., "Source Separation from Multiple Microphone Measurements in the Far Field of a Full Scale Aero Engine," Tech. Rep. AIAA-2008-2809, AIAA, 2008.

[66]Weir, D. S. and Mendoza, J. M., "Baseline Noise Measurements from the Engine Validation of Noise and Emissions Reduction Technology Program," Tech. Rep. AIAA-2008-2807, AIAA, 2008.

[67]Schuster, B., "Statistical Considerations for Gas Turbine Engine Noise Measurements," Tech. Rep. AIAA-2008-2808, AIAA, 2008.

[68]Royalty, C. M. and Schuster, B., "Noise from a Turbofan Engine Without a Fan from the Engine Validation of Noise and Emission Reduction Technology (EVNERT) Program," Tech. Rep. AIAA-2008-2810, AIAA, 2008.

[69]Dougherty, R. P. and Mendoza, J. M., "Phased Array Beamforming with 100-foot Polar Arc Microphones in a Static Engine Noise Test," Tech. Rep. AIAA-2008-51, AIAA, 2008.

[70]Dougherty, R. P. and Mendoza, J. M., "Nacelle In-duct Beamforming using Modal Steering Vectors," Tech. Rep. AIAA-2008-2812, AIAA, 2008.

[71]Hultgren, L. and Miles, J., "Noise-Source Separation Using Internal and Far-Field Sensors for a Full-Scale Turbofan Engine," AIAA-2009-3220, May 2009, 15th AIAA/CEAS Aeroacoustics Conference, Miami, FL, May 11-13, 2009.

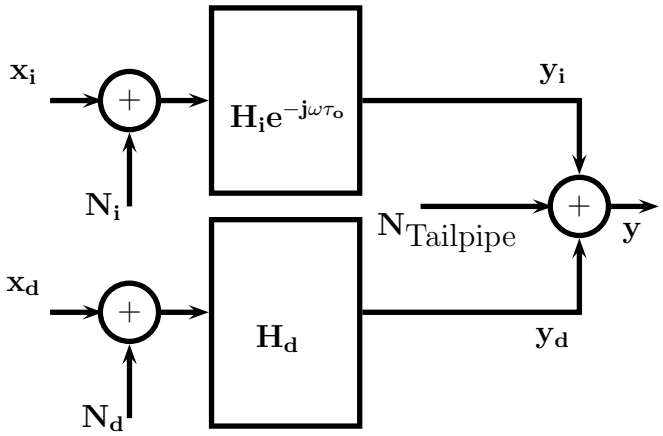

Figure 1. Turbine-Combustor-Tailpipe Noise System

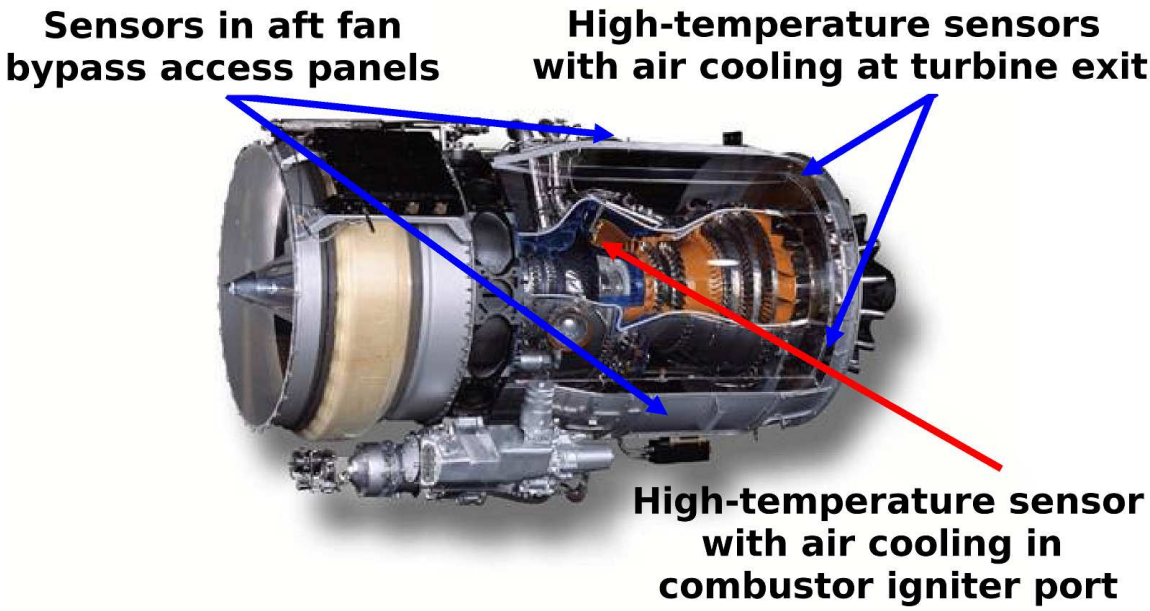

Figure 2. Honeywell TECH977 engine.

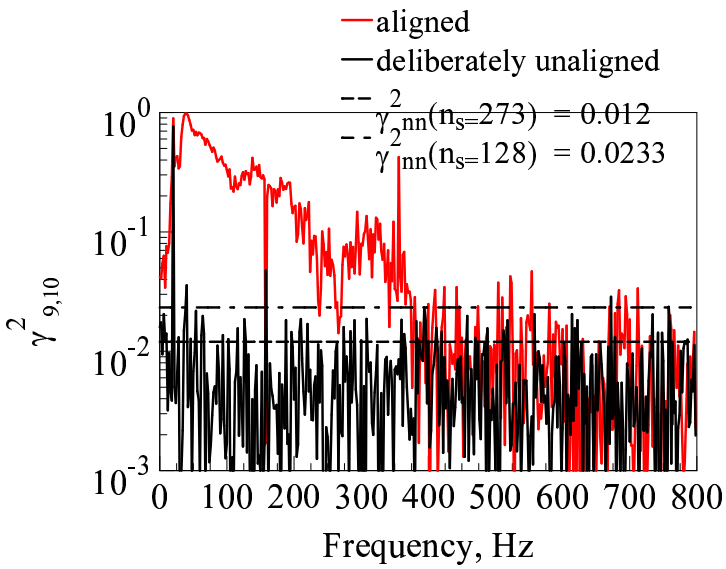

(a) Coherence

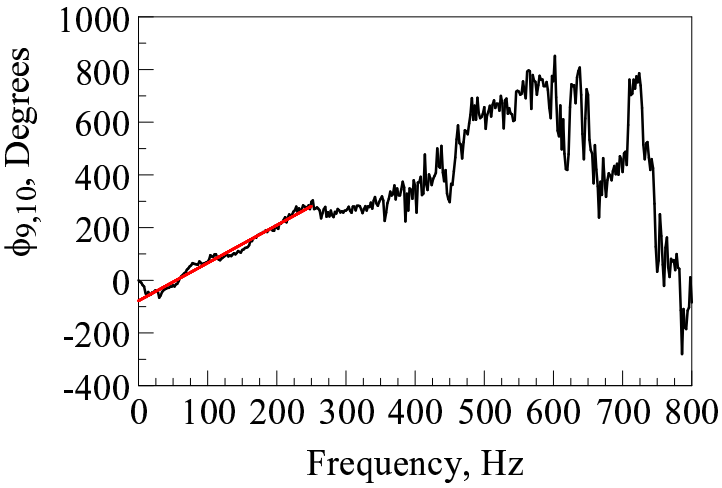

(b) Cross-spectrum phase angle

Figure 3. Post-combustion residence time at 48 percent maximum power using sensors CIP1(9) and T551(10) is 3.99 ms ($\phi_{9,10} = 3.99\frac{360}{1000}f - 78.0678°$).

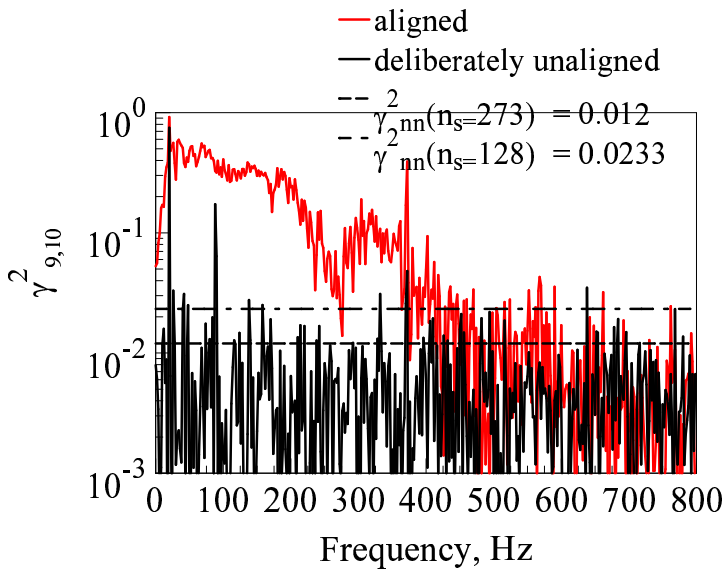

(a) Coherence

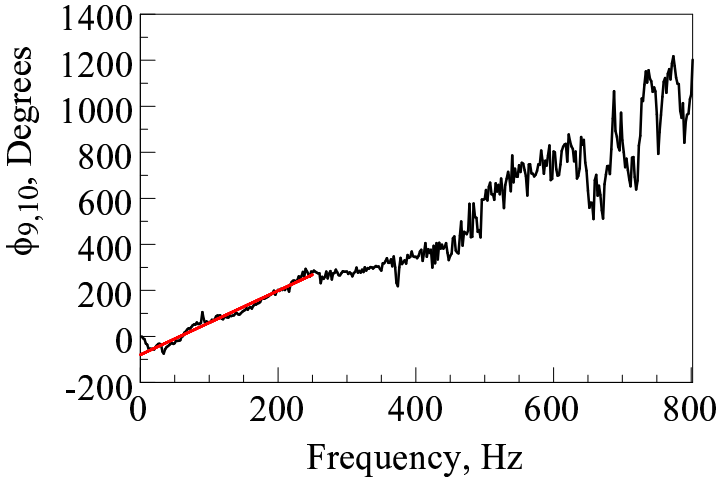

(b) Cross-spectrum phase angle

Figure 4. Post-combustion residence time at 54 percent maximum power using sensors CIP1(9) and T551(10) is 3.867 ms ($\phi_{9,10} = 3.867\frac{360}{1000}f - 79.9248°$).

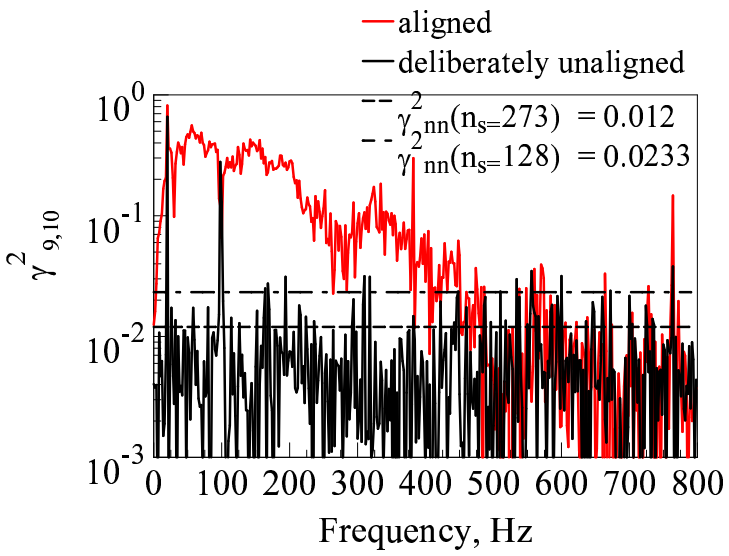

(a) Coherence

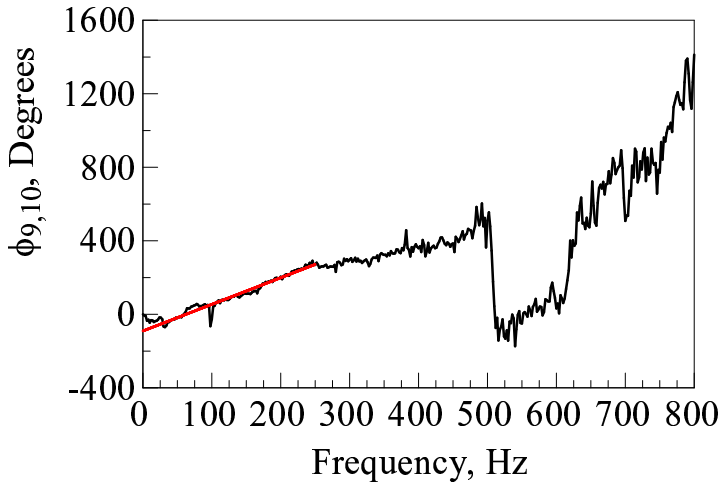

(b) Cross-spectrum phase angle

Figure 5. Post-combustion residence time at 60 percent maximum power using sensors CIP1(9) and T551(10) is 4.0229 ms ($\phi_{9,10} = 4.0229\frac{360}{1000}f - 90.7813°$).

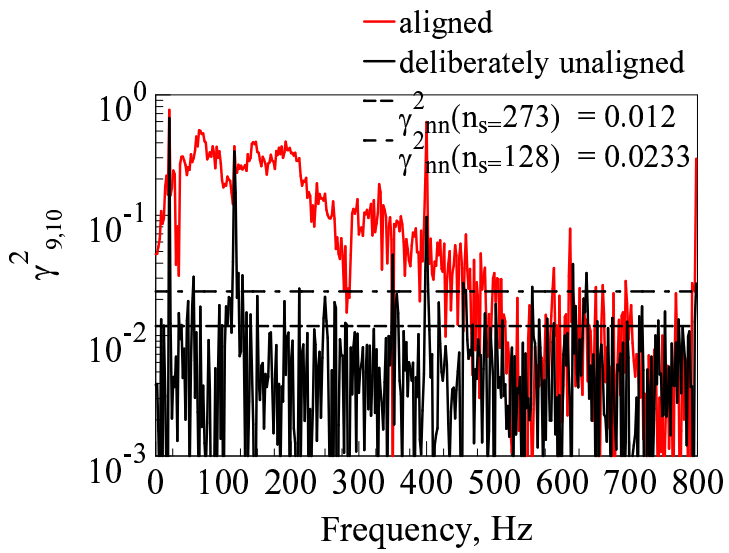

(a) Coherence

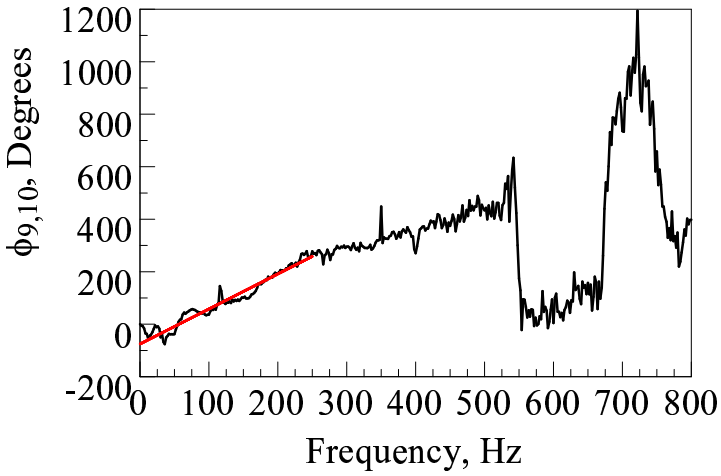

(b) Cross-spectrum phase angle

Figure 6. Post-combustion residence time at 71 percent maximum power using sensors CIP1(9) and T551(10) is 3.7079 ms ($\phi_{9,10} = 3.7079\frac{360}{1000}f - 75.5638°$).

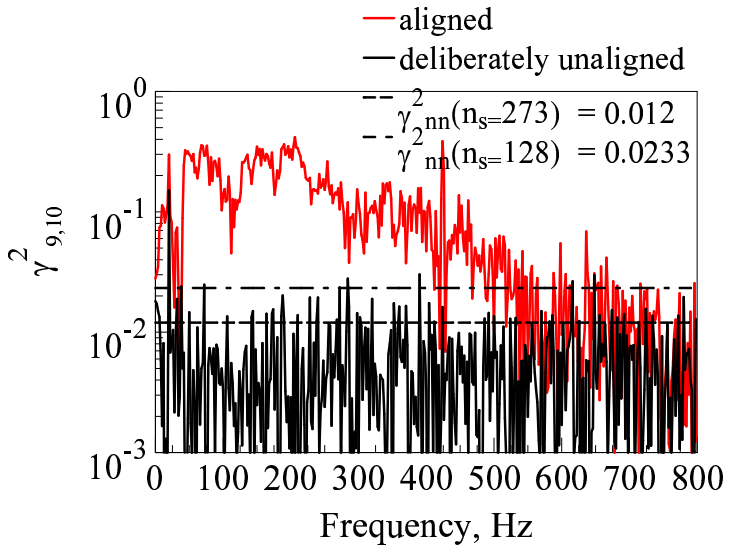

(a) Coherence

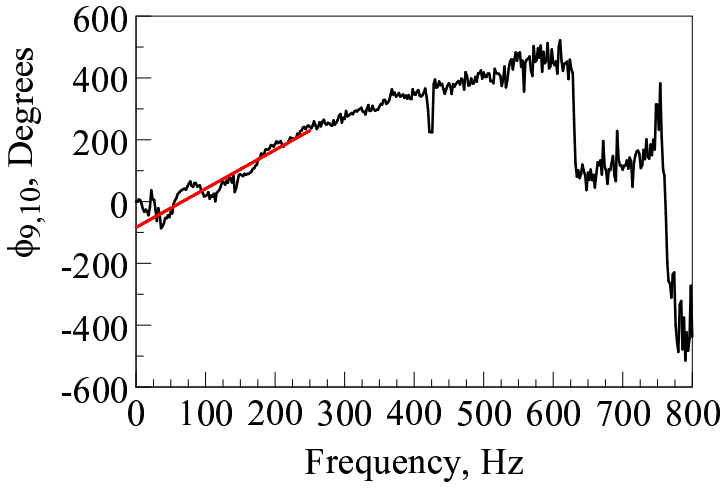

(b) Cross-spectrum phase angle

Figure 7. Post-combustion residence time at 87 percent maximum power using sensors CIP1(9) and T551(10) is 3.4814 ms ($\phi_{9,10} = 3.4814\frac{360}{1000}f - 83.7381°$).

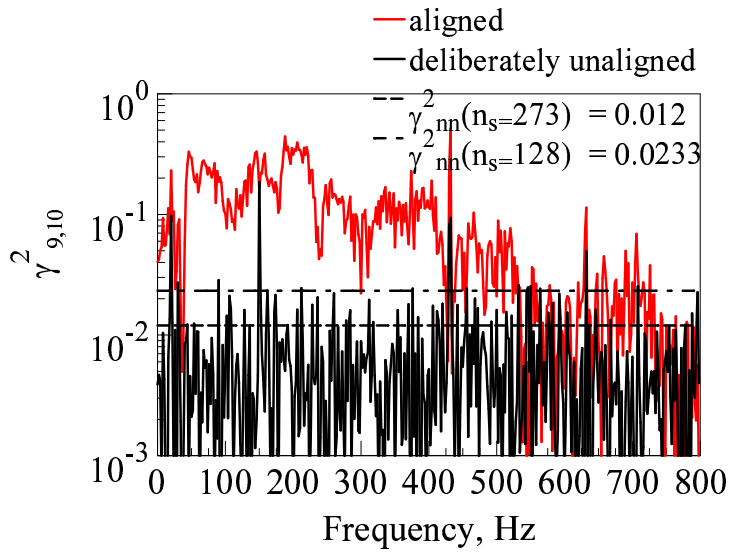

(a) Coherence

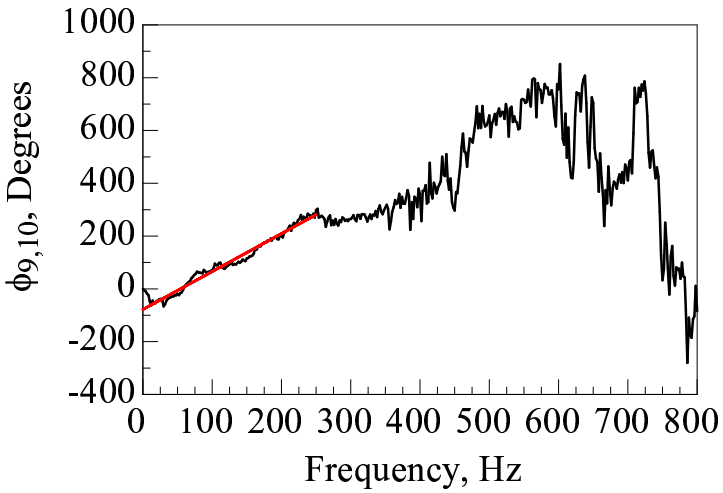

(b) Cross-spectrum phase angle

Figure 8. Post-combustion residence time at 98 percent maximum power using sensors CIP1(9) and T551(10) is 3.99 ms ($\phi_{9,10} = 3.99\frac{360}{1000}f - 78.0678°$).

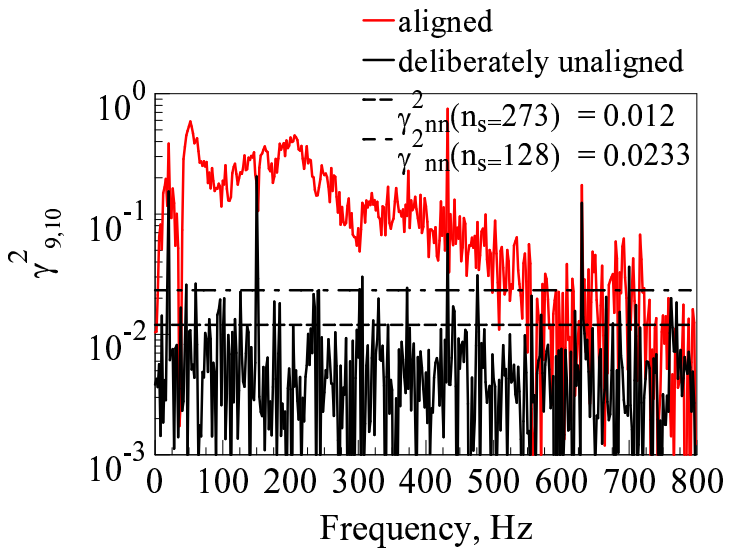

(a) Coherence

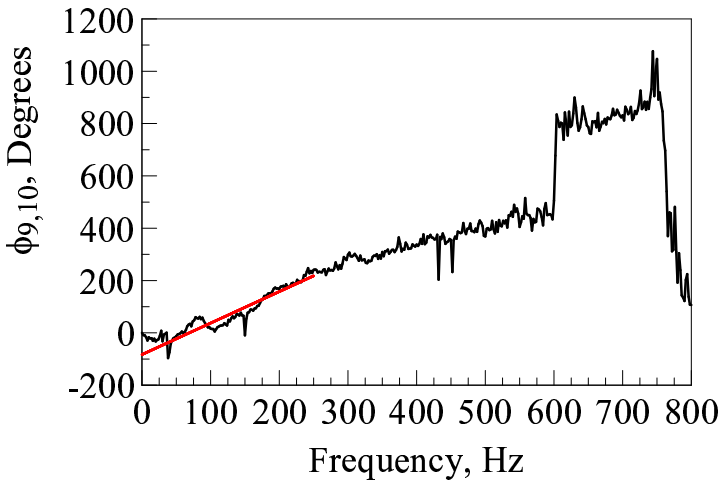

(b) Cross-spectrum phase angle

Figure 9. Post-combustion residence time at 99 percent maximum power using sensors CIP1(9) and T551(10) is 3.3435 ms ($\phi_{9,10} = 3.3435\frac{360}{1000}f - 83.0246°$).

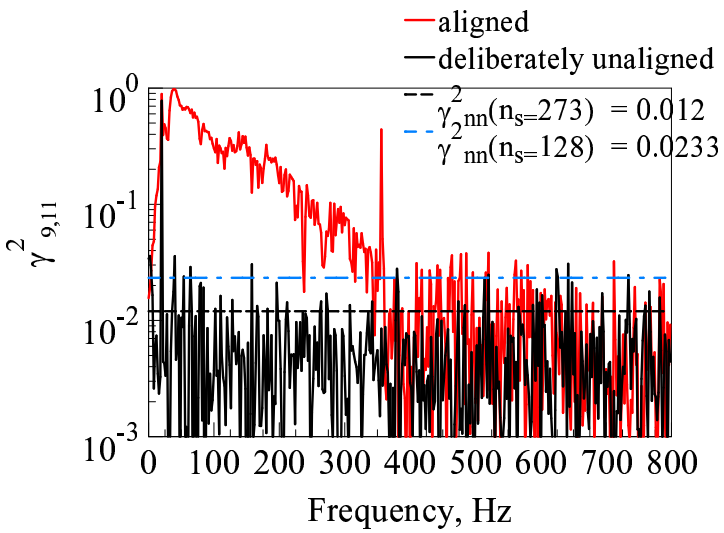

(a) Coherence

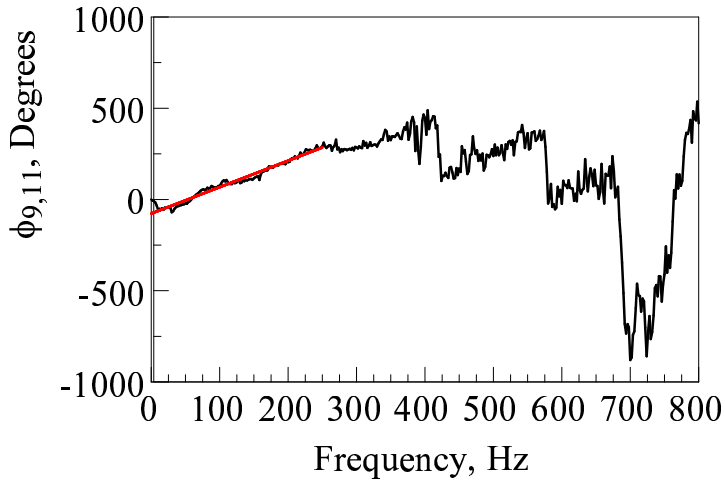

(b) Cross-spectrum phase angle

Figure 10. Post-combustion residence time at 48 percent maximum power using sensors CIP1(9) and T552(11) is 4.024 ms ($\phi_{9,11} = 4.024\frac{360}{1000}f - 77.3482°$).

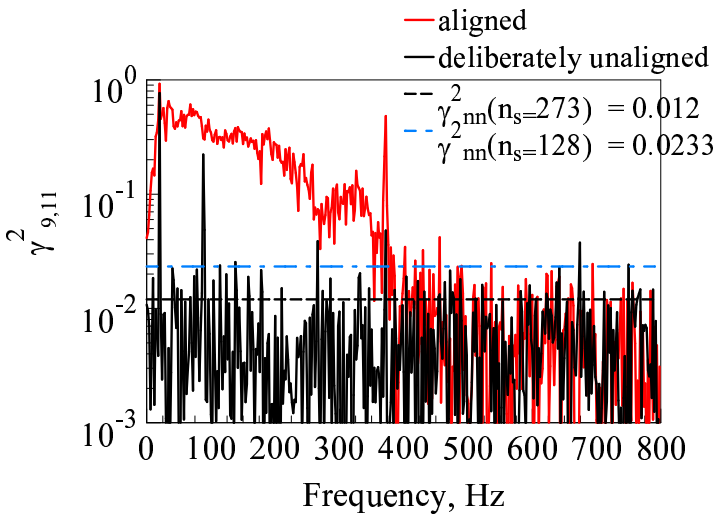

(a) Coherence

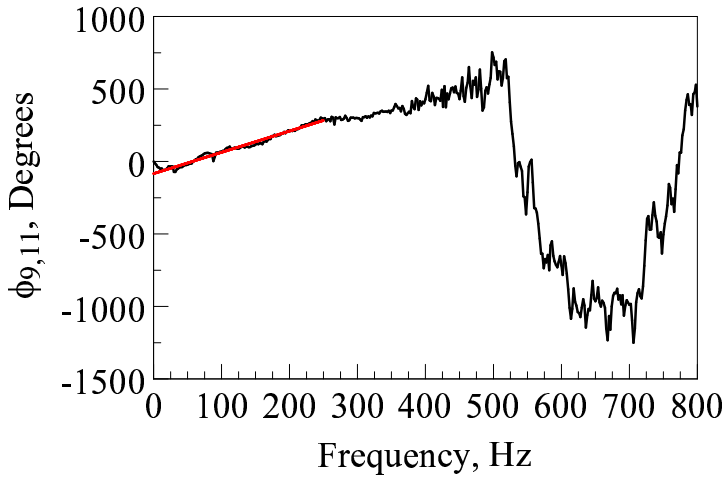

(b) Cross-spectrum phase angle

Figure 11. Post-combustion residence time at 54 percent maximum power using sensors CIP1(9) and T552(11) is 4.0664 ms ($\phi_{9,11} = 4.0664\frac{360}{1000}f - 83.6347°$)**.**

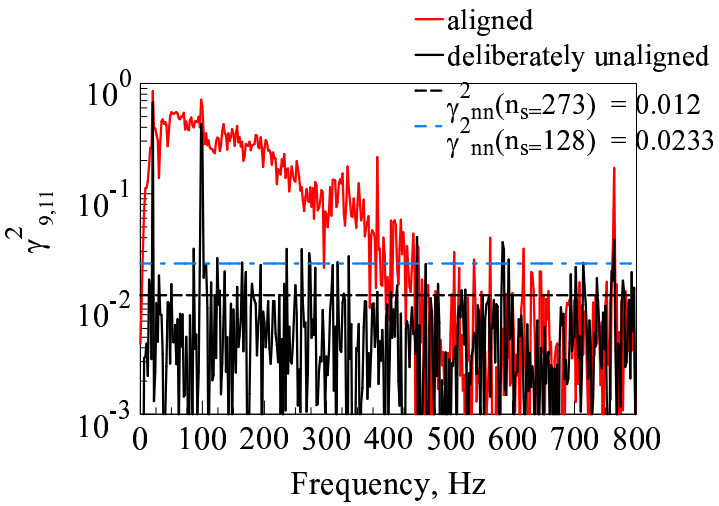

(a) Coherence

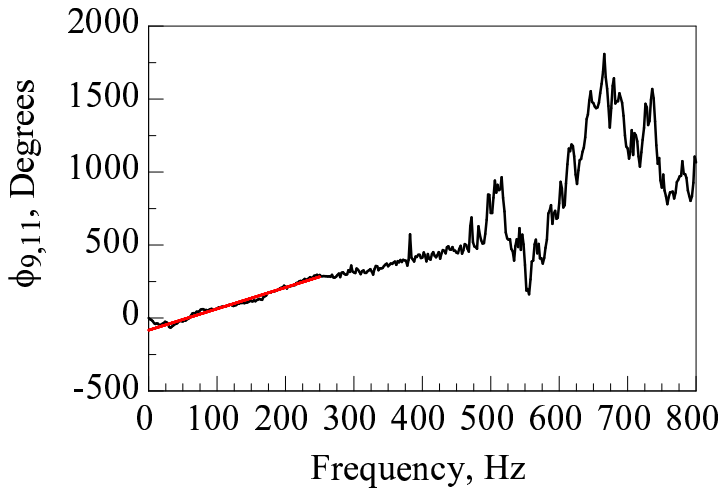

(b) Cross-spectrum phase angle

Figure 12. Post-combustion residence time at 60 percent maximum power using sensors CIP1(9) and T552(11) is 4.0664 ms ($\phi_{9,11} = 4.0664\frac{360}{1000}f - 83.6347°$).

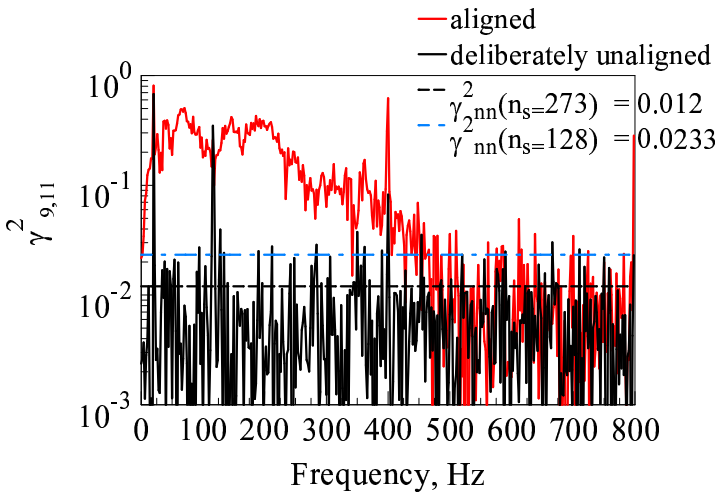

(a) Coherence

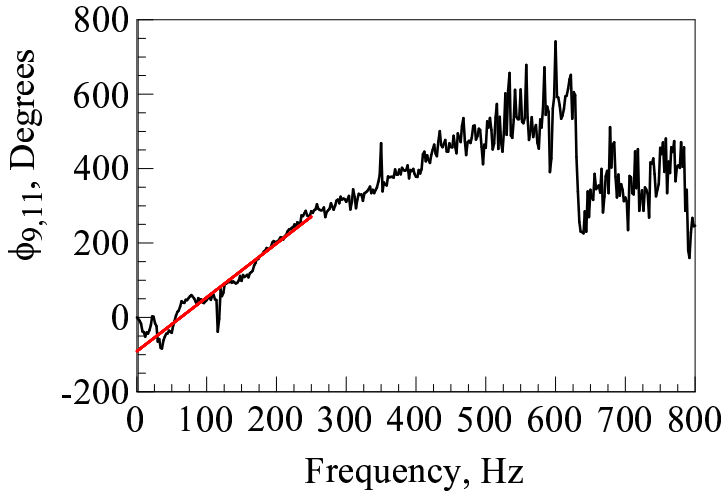

(b) Cross-spectrum phase angle

Figure 13. Post-combustion residence time at 71 percent maximum power using sensors CIP1(9) and T552(11) is 4.0188 ms ($\phi_{9,11} = 4.0188\frac{360}{1000}f - 90.96°$).

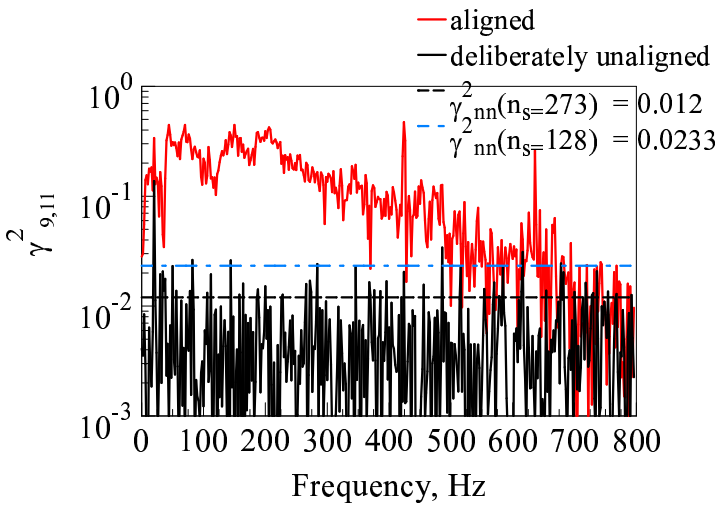

(a) Coherence

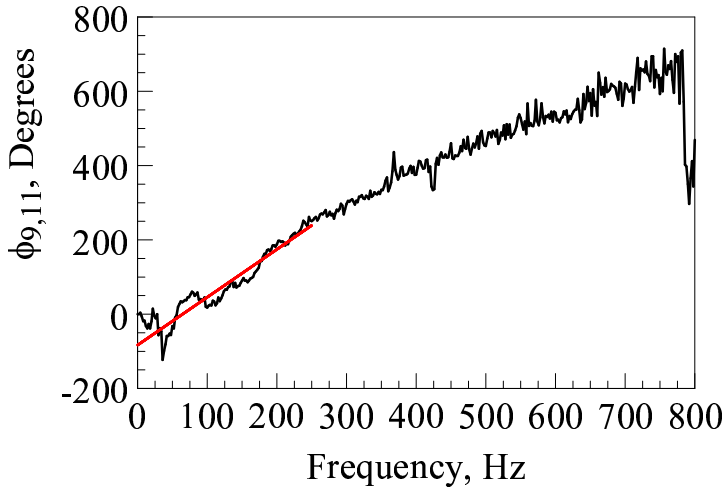

(b) Cross-spectrum phase angle

Figure 14. Post-combustion residence time at 87 percent maximum power using sensors CIP1(9) and T552(11) is 3.5794 ms ($\phi_{9,11} = 3.5794\frac{360}{1000}f - 83.3152°$).

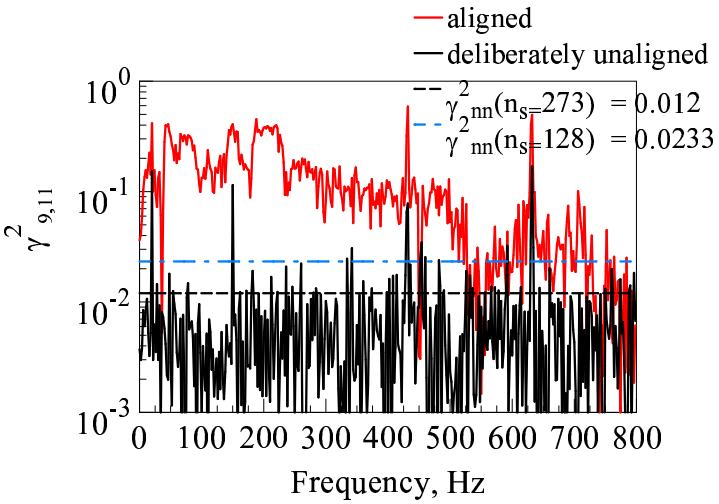

(a) Coherence

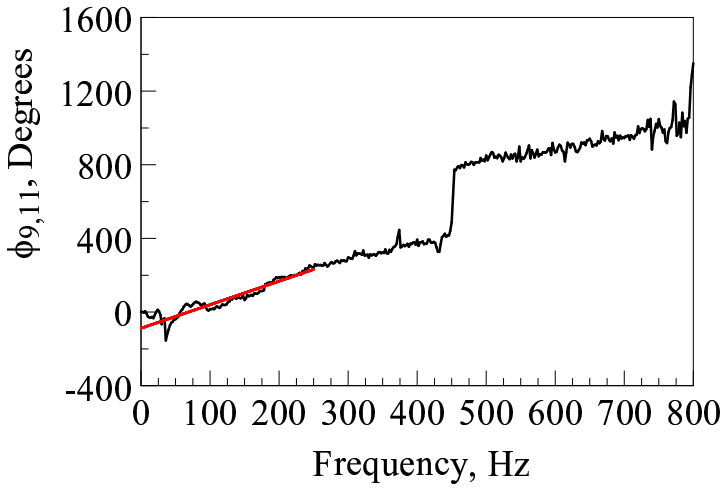

(b) Cross-spectrum phase angle

Figure 15. Post-combustion residence time at 98 percent maximum power using sensors CIP1(9) and T552(11) is 3.99 ms ($\phi_{9,11} = 3.5477\frac{360}{1000}f - 88.01°$).

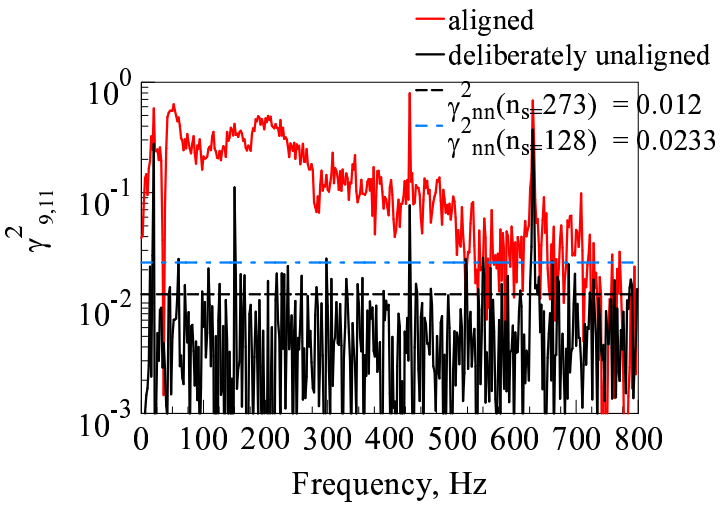

(a) Coherence

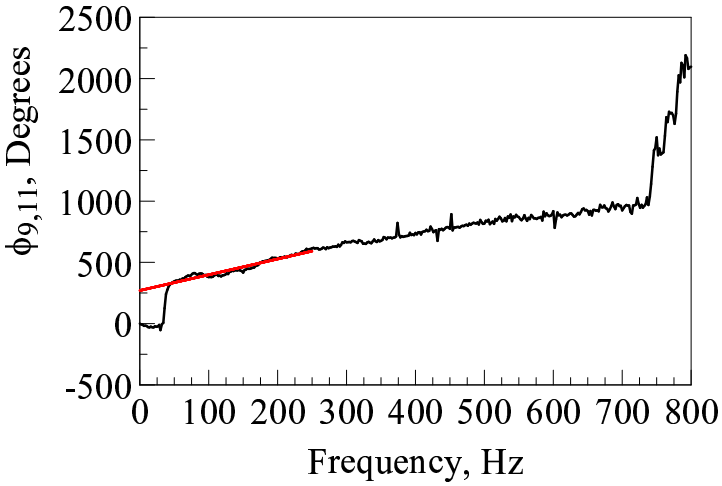

(b) Cross-spectrum phase angle

Figure 16. Post-combustion residence time at 99 percent maximum power using sensors CIP1(9) and T552(11) is 3.5703 ms. ($\phi_{9,11} = 3.5703\frac{360}{1000}f270.4594°$)

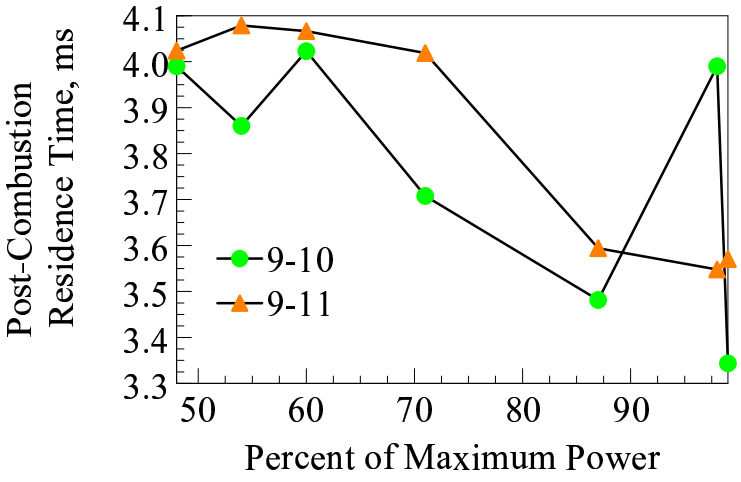

Figure 17. Post-combustion residence time at various maximum power settings.)